

The fate of close encounters between binary stars and binary supermassive black holes

Yi-Han Wang^{1*}, Nathan Leigh², Ye-Fei Yuan^{3,4}, Rosalba Perna¹

¹ *Department of Physics and Astronomy, Stony Brook University, Stony Brook, NY 11794-3800, USA*

² *Department of Astrophysics, American Museum of Natural History, Central Park West and 79th Street, New York, NY 10024*

³ *Department of Astronomy, University of Science and Technology of China, Hefei, Anhui 230026, China*

⁴ *CAS Key Laboratory for Research in Galaxies and Cosmology, Hefei, Anhui 230026, China*

25 December 2017

ABSTRACT

The evolution of main sequence binaries that reside in the Galactic Centre can be heavily influenced by the central super massive black hole (SMBH). Due to these perturbative effects, the stellar binaries in dense environments are likely to experience mergers, collisions or ejections through secular and/or non-secular interactions. More direct interactions with the central SMBH are thought to produce hypervelocity stars (HVSs) and tidal disruption events (TDEs). In this paper, we use N-body simulations to study the dynamics of stellar binaries orbiting a central SMBH primary with an outer SMBH secondary orbiting this inner triple. The effects of the secondary SMBH on the event rates of HVSs, TDEs and stellar mergers are investigated, as a function of the SMBH-SMBH binary mass ratio. Our numerical experiments reveal that, relative to the isolated SMBH case, the TDE and HVS rates are enhanced for, respectively, the smallest and largest mass ratio SMBH-SMBH binaries. This suggests that the observed event rates of TDEs and HVSs have the potential to serve as a diagnostic of the mass ratio of a central SMBH-SMBH binary. The presence of a secondary SMBH also allows for the creation of hypervelocity binaries. Observations of these systems could thus constrain the presence of a secondary SMBH in the Galactic Centre.

Key words: black hole physics-Galaxy:numerical-stellar dynamics

1 INTRODUCTION

Supermassive black holes (SMBHs) ubiquitously reside at the centres of galaxies (e.g., Kormendy & Ho 2013). Observations show that, in the inner ~ 1 parsec (pc) of our own Milky Way, the gravitational potential is dominated by a central SMBH with mass $\sim 4 \times 10^6 M_{\odot}$ (e.g., Alexander 2005; Gillessen et al. 2017). In the immediate vicinity of the SMBH, there exists a densely packed and complicated stellar environment. The relatively high stellar density at the center of the Milky Way and the small mass of the SMBH imply that the relaxation time of two-body interaction could be as short as a Gyr, but longer estimates have also been quoted (e.g. Merritt 2013).

Much uncertainty persists in understanding the constituents of this inner Keplerian-dominated region. Some parameter space exists that permits for the presence of an IMBH with mass 10^3 - $10^4 M_{\odot}$ (Yu & Tremaine 2003; Gualandris, Portegies Zwart & Sapior 2005; Gualandris &

Merritt 2009). A handful of compact binary star systems have also been observed in the Galactic Centre (Martins et al. 2006). These bound state binaries orbiting the central SMBH form hierarchical triple systems, and are hence subject to both secular dynamical effects and chaotic perturbations from other objects (e.g. Antonini et al. 2010; Leigh et al. 2016a). This has the potential to stimulate a high rate of observable dynamical phenomena, such as hypervelocity stars and tidal disruption events.

Gravitational encounters involving stellar binaries and an SMBH operating on characteristic timescales shorter than the secular timescale have been studied extensively: (i) When the stellar binaries are on low angular momentum orbits, the stellar binaries are considered to be easily broken up due to the strong tidal field of the SMBH. As a result, one component is captured by the SMBH, while the other is ejected at high velocity. This is one mechanism believed to produce hypervelocity stars (HVSs) (e.g., Hills 1988; Yu & Tremaine 2003; Antonini et al. 2010); (ii) Conversely, the stars in a binary can be tidally disrupted by the SMBH if the relative distance is less than the tidal disruption radius of a given binary component. The subsequent accretion of

* E-mail:rosalba.perna@stonybrook.edu;
yihan.wang.1@stonybrook.edu

the stellar debris by the SMBH results in a strong flare of electromagnetic radiation, called to a tidal disruption event (TDE) (e.g., Hills 1975; Rees 1988; Phinney 1989; Gezari et al. 2012; Mandel & Levin 2015); (iii) Finally, such a close interaction between the SMBH and the stellar binary may lead to a physical collision between the two components of the binary (e.g., Ginsburg & Loeb 2007).

If the orbital plane of the stellar binary is inclined relative to the plane of its orbit about the SMBH by $\gtrsim 40^\circ$, the eccentricity and inclination of the binary orbit will experience periodic oscillations on a secular timescale, known as Lidov-Kozai (LK) oscillations (e.g., Lidov 1962; Kozai 1962). Here, the orbital eccentricity of the binary slowly increases while the inclination decreases, conserving angular momentum, and vice versa. The effects of LK oscillations include the formation of a number of exotic astrophysical systems (e.g., Eggleton & Kiseleva-Eggleton 2001; Fabrycky & Tremaine 2007; Holman, Touma, & Tremaine 1997; Innanen et al. 1997; Wu & Murray 2003; Storch, Anderson, & Lai 2014; Liu, Lai, & Yuan 2015; Anderson, Storch, & Lai 2016). For example, the presence of a central massive BH can accelerate the rate of black hole binary mergers due LK oscillations, both at the centres of galaxies and globular clusters (e.g., Blaes et al. 2002; Miller & Hamilton 2002; Wen 2003; Antonini, Murray & Mikkola 2014; Fragione, Ginsburg, & Kocsis 2017). Similarly, LK oscillations can stimulate Type Ia supernova from white-dwarf binary mergers (e.g., Thompson 2011; Prodan, Murray, & Thompson 2013) or direct collisions between main-sequence stars and hence blue straggler formation (e.g., Katz & Dong 2012; Kushnir et al. 2013; Leigh et al. 2016b). An enhanced rate of stellar TDEs might also be expected in the presence of a massive BH, due to the eccentric LK mechanism alone (e.g., Li et al. 2015; Liu, Wang, & Yuan 2017).

In this paper, we consider stellar binaries orbiting around a central primary SMBH, perturbed by a distant secondary SMBH. We study the effects of different mass ratios q of the SMBH-SMBH binary in determining the relative rates of HVS production, TDE production and binary mergers. The presence of a secondary SMBH orbiting the inner SMBH-binary star triple serves to perturb and/or accelerate the secular dynamical evolution of the inner triple system.

The SMBH-SMBH binary, together with the stellar binary, can be decomposed into two separate hierarchical triple systems. These are the SMBH-star-star triple and the SMBH-stellar binary-SMBH triple. As anticipated, the secular dynamical processes in the inner triple are accelerated by the presence of the secondary SMBH, leading to an enhancement in the overall rate of observable astronomical events (TDEs, HVSs, mergers). When the inner triple has a relative orbital inclination that lies in the range $40^\circ \sim 140^\circ$, LK oscillations occur. Subsequently, the eccentricity of the stellar binary can be excited, leading to a merger between the two binary components. Conversely, when LK oscillations in the outer triple are operating, the stellar binary orbit about the primary SMBH can be excited to very high eccentricities. If the periastron distance corresponding to this orbit reaches the tidal disruption radius, the binary will be disrupted, producing a TDE and/or an HVS. The mass of the secondary SMBH plays a fundamental role in this four-body system, by affecting the time scales for LK oscillations to operate.

Our paper is organized as follows. In Section 2, we introduce the geometry of the four-body system. Through a comparison of the relevant timescales, we characterize the parameter space where outer LK oscillations dominate over inner LK oscillations and vice versa. In Section 3, we describe the numerical setup and initial conditions for our N-body simulations. In Section 4, we present the results of our N-body simulations, and explore the evolution of stellar binaries orbiting inside the orbit of an SMBH-SMBH binary as a function of its mass ratio. Our conclusions are summarized in Section 5.

2 A STELLAR BINARY ORBITING AN SMBH BINARY

As shown in Figure 1, we label the masses of the stars by m_{*1} and m_{*2} (i.e., the stellar binary components), the mass of the primary SMBH by m_1 , and the mass of the secondary SMBH by m_2 . For the orbital parameters, we use $a_{*,\text{CM},\text{BH}}$ to denote the semi-major axes, $e_{*,\text{CM},\text{BH}}$ the eccentricities and $r_{*,\text{CM},\text{BH}}$ the separations between the two components of each binary. Here, the subscripts “*, CM, BH” denote, the (internal) orbit of the stellar binary, the orbit of the stellar binary about the primary SMBH and the orbit of the secondary SMBH about the primary SMBH, respectively. Geometrically, the four-body system can be decomposed in to an inner triple (SMBH-star-star) and an outer triple (SMBH-stellar binary-SMBH). In each triple system, if the inclination between two orbital planes is $> 40^\circ$ and $< 140^\circ$, then the eccentricity and inclination of the inner orbit will experience periodic oscillations on a secular timescale, known as Lidov-Kozai (LK) oscillations (e.g., Lidov 1962; Kozai 1962). If the outer BH is on a highly inclined orbit around the binary and at a moderate distance, the LK oscillations breakdown. Non-secular and chaotic effects will be introduced into the system, which have the potential to lead to a rapid merger in the inner orbit (Antonini, Murray, & Mikkola 2014). In such a four-body system, the competition between LK resonances in the inner and outer triple configurations, together with non-secular and chaotic effects, could serve as an important catalyst for astronomically observable events such as the production of HVSs, TDEs and stellar mergers.

2.1 Basic relations

Several physical mechanisms play a fundamental role in our simulations. They are summarized in the following:

- (i) Due to their low densities, main-sequence stars are easily tidally disrupted in the vicinity of an SMBH. Tidal disruption occurs for stars that approach the SMBH more closely than r_{*t} ,

$$r_{*t} \sim \left(\frac{m_{\text{SMBH}}}{m_*} \right)^{1/3} R_* \quad (1)$$

where m_{SMBH} is the mass of the SMBH, m_* the mass of the star and R_* the radius of the star. In our simulations, we use the mass-radius relation $R_*/R_\odot = (m_*/m_\odot)^{0.75}$ which yields $R_* = 0.01\text{AU}$ for $m_* = 3m_\odot$ (e.g., Hansen, Kawaler, & Trimble 2004).

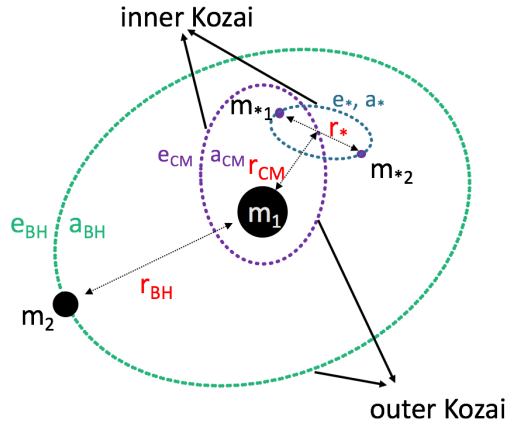


Figure 1. Schematic illustration of the two triple systems in our four-body system. The first triple consists of the primary SMBH m_1 and the stellar binary $m_{*,1}, m_{*,2}$. The second triple consists of the primary SMBH m_1 , the centre of mass of the stellar binary and the second SMBH m_2 .

(ii) Stellar binaries will be broken apart by the SMBH if the stellar binary enters the tidal breakup radius r_{bt} ,

$$r_{bt} \sim \left(\frac{m_{\text{SMBH}}}{m_{*1} + m_{*2}} \right)^{1/3} r_* \quad (2)$$

where r_* is the separation of the two components in the stellar binary.

(iii) The stellar binary remains bound to the black hole within the Hill sphere of the primary SMBH (m_1). The radius of the Hill sphere is

$$R_{\text{Hill}} = a_{\text{BH}}(1 - e_{\text{BH}}) \left(\frac{m_1}{3m_2} \right)^{1/3} \quad (3)$$

For stellar binaries within the Hill sphere, there is no chance either of tidal disruption by the secondary SMBH (m_2) or of being ejected from the system by the slingshot effect induced by the secondary SMBH (m_2). For large mass ratios of the SMBH binary, the stellar binaries could reside outside of the Hill sphere. For these stellar binaries, the hierarchical structure of the four-body system will be broken. The LK oscillations can no longer operate and affect the internal system evolution.

(iv) The hierarchical condition for a stable triple system is

$$\varepsilon_{\text{oct}} \equiv \frac{a_{\text{CM}}}{a_{\text{BH}}} \frac{e_{\text{BH}}}{1 - e_{\text{BH}}^2} < 0.1 \quad (4)$$

For binaries whose orbital parameters satisfy this hierarchical condition, the LK effect can excite the binary orbit. This could ultimately lead to decoupling of the binary followed by tidal disruptions, mergers, or HVSs. At the quadrupole level, the LK effect defines the maximum value of the excited eccentricity to be $e_{\text{max}} = \sqrt{1 - \frac{5}{3} \cos^2 i_{\text{int}}}$, where i_{int} is the initial inclination between the inner and outer orbital planes of the triple system. Combining this with Eq (1) and the stellar mass-radius relation, we can calculate analytically the rates of single TDEs and mergers.

For those binaries that do not satisfy the hierarchical con-

dition, a chaotic effect is introduced into the system. Nevertheless, scattering experiments reveal that the binary orbit can still be excited in the strong interaction region where $r_{\text{CM}} \sim [0.5, 2]a_{\text{BH}}$ (e.g., Chen et al. 2009).

(v) The hardening radius of the black hole binary is

$$a_h = \frac{Gm_2}{4\sigma_*^2} \quad (5)$$

where σ_* is the velocity dispersion of the stellar cusp surrounding the primary SMBH.

2.2 Time scales

In order to identify the parameter space where the Lidov-Kozai effect becomes dominant, we consider the different sources of apsidal precession in galactic nuclei hosting SMBHs. For the inner triple system, the stellar binary is immersed in a dense environment. Other perturbative effects may come into play and affect the evolution of the stellar binary, or even change the outcome of an otherwise secular interaction.

Binaries orbited by a highly inclined perturber will undergo LK oscillations. In the inner triple, the corresponding timescale at the approximation of the quadrupole level is (e.g., Lidov 1962; Kozai 1962)

$$T_{\text{K,B}} = \frac{1}{n_*} \left(\frac{m_{*1} + m_{*2}}{m_1} \right) \left(\frac{a_{\text{CM}}}{a_*} \right)^3 (1 - e_{\text{CM}}^2)^{3/2} \quad (6)$$

where $n_* = \sqrt{G(m_{*1} + m_{*2})/a_*^3}$ is the mean motion of the stellar binary.

Similarly, in the outer triple, the corresponding timescale at the quadrupole level is

$$T_{\text{K,C}} = \frac{1}{n_{\text{CM}}} \left(\frac{m_{*1} + m_{*2} + m_1}{m_2} \right) \left(\frac{a_{\text{BH}}}{a_{\text{CM}}} \right)^3 (1 - e_{\text{BH}}^2)^{3/2} \quad (7)$$

where $n_{\text{CM}} = \sqrt{G(m_{*1} + m_{*2} + m_1)/a_{\text{CM}}^3}$ is the mean motion of the stellar binary orbiting the primary SMBH.

If the stellar binary orbital separation at pericentre is sufficiently small, additional effects such as general relativity (GR) can dominate the tidal torque exerted by the outer binary, suppressing the excitation of its eccentricity (e.g., Blaes et al. 2002; Naoz et al. 2013a; Naoz 2016). The timescale for precession of the argument of periapsis caused by the first order post Newtonian (PN) correction in the inner and outer orbits is

$$T_{\text{GR,*}} = \frac{2\pi c^2}{3G^{3/2}} \frac{a_*^{5/2}(1 - e_*^2)}{(m_{*1} + m_{*2})^{3/2}} \quad (8)$$

and

$$T_{\text{GR,CM}} = \frac{2\pi c^2}{3G^{3/2}} \frac{a_{\text{CM}}^{5/2}(1 - e_{\text{CM}}^2)}{(m_{*1} + m_{*2} + m_1)^{3/2}} \quad (9)$$

respectively. The interaction between the inner and outer binaries at 1 PN order adds an additional term in the equation of motion. The related timescale is given by (e.g., Naoz et al. 2013a; Will 2014a,b)

$$T_{\text{GR,int}} = \frac{16c^2 a_{\text{CM}}^3}{9G^{3/2} a_*^{1/2} e_* (1 - e_*^2)^{1/2}} \times \frac{(m_{*1} + m_{*2})^{3/2}}{(m_{*1}^2 + m_{*1}m_{*2} + m_{*2}^2)m_1} \quad (10)$$

Figure 2 shows a comparison of the timescales in an illustrative example: $m_{*1} = 3M_{\odot}$, $m_{*2} = 3M_{\odot}$ and $m_1 = 4 \times 10^6 M_{\odot}$ with different sets of mass ratio and eccentricity of the binary SMBH.

We ran our simulations with input parameters indicated with orange lines in Figure 2. In this region, at $a_{\text{BH}} \sim 0.01\text{pc}$, it is clearly shown in all four panels that both $T_{GR,*}$ and $T_{GR,\text{CM}}$ are much longer than $T_{\text{K,B}}$. This means that GR precession of the orbits is totally suppressed by the inner LK oscillations at any point in the parameter space we consider. Therefore, GR can be neglected in these simulations. The lower-middle inset in the lower two panels indicates that GR precession of the stellar binary centre of mass orbit dominates over the outer LK oscillations. Thus, for small mass ratios, post-Newtonian terms must be included in these simulations. The upper left-most inset in the upper two panels indicates that, for large mass ratios, the inner and outer LK oscillations compete with each other. This can serve as a catalyst for the occurrence of a number of interesting astronomical events, such as TDEs, HVSs and mergers. Conversely, in the lower two panels with small mass ratios, the outer LK oscillations are completely suppressed by the inner LK oscillations. In this case, stellar mergers become the dominant event in our simulations.

3 INITIAL MODELS AND NUMERICAL METHODS

In this section, we describe the numerical method used in this paper, and present the orbital parameters and initial conditions considered for the target four-body system.

3.1 Numerical Method

We use N -body simulations to study the evolution of main sequence binaries in the Galactic Centre. In each simulation, a stellar binary orbits the central SMBH, which is in turn orbited by a remote less-massive SMBH. All the simulations were carried out using the code NBODY, developed by ourselves. In this code, we use the Position Extended Forest-Ruth Like (PEFRL) integrator with adaptive time stepping. The PEFRL algorithm is a fourth-order symplectic numerical method. Unlike other algorithms, the symplectic method conserves the constants of motion (i.e., total energy E and total angular momentum L) in Hamiltonian systems over long integration times. We test the performance of several integrators using our N -body code by adopting the same set of initial conditions, performing the same simulations and comparing the results. As expected, symplectic methods perform better than non-symplectic methods (see the Appendix A for more details).

To ensure reasonable integration times, we do not use the regular adaptive time stepping control strategy, since this requires the higher-order error estimation embedded in the PEFRL algorithm. Instead, we adopt the time-step criterion in the cosmology code GADGET-2 (e.g., Springel 2005):

$$\Delta t_{\text{grav}} = \max \left\{ \Delta t_{\text{min}}, \sqrt{\frac{\eta}{|a_{\text{min}}(t)|}} \right\}, \quad (11)$$

where Δt_{min} is the minimal time-step allowed in the system,

to avoid an infinite shrinking of the time-step. η is a user-chosen accuracy parameter and $|a_{\text{min}}(t)|$ gives the minimal acceleration among all the particles in the system at any given time t . This time-step criterion is only dependent on the current status of the system. Thus, additional integration time is not needed to perform higher-order estimations. In our chosen problem, given the initial total energy of the system $E(t=0)$, the PEFRL method controls the energy fluctuation $|\frac{E(t)-E(0)}{E(0)}|$ to remain within the range 10^{-11} - 10^{-13} , assuming $\eta = 0.1R_{\odot}$.

The equation of motion is determined by the Newtonian gravitational acceleration, including post-Newtonian terms up to 2.5th order

$$\mathbf{a}_i = \mathbf{a}_{\text{N},i} + \mathbf{a}_{\text{PN},i}, \quad (12)$$

where $a_{\text{N},i}$ is the Newtonian acceleration imparted to the i -th particle

$$\mathbf{a}_{\text{N},i} = - \sum_{j \neq i} \frac{Gm_j}{r_{ij}^3} \mathbf{n} \quad (13)$$

and $\mathbf{n} = \mathbf{r}_i - \mathbf{r}_j$ above is the direction vector.

Post-Newtonian terms up to 2.5th order (Soffel 1989) are included in the equation of motion in those areas of parameter space in Fig.2 for which the effects due to GR are important. Otherwise, we set $a_{\text{PN},i}$ to zero in our simulations.

$$\mathbf{a}_{\text{PN},i} = c^{-2} \mathbf{a}_{1\text{PN},i} + c^{-4} \mathbf{a}_{2\text{PN},i} + c^{-5} \mathbf{a}_{2.5\text{PN},i} \quad (14)$$

where $\mathbf{a}_{1\text{PN},i}$, $\mathbf{a}_{2\text{PN},i}$ and $\mathbf{a}_{2.5\text{PN},i}$ represent the 1st-order, 2nd-order and 2.5th-order terms, respectively (e.g., Kupi, Amaro-Seoane, & Spurzem 2006). Since the full equation is very long, we are not going to expand it here.

3.2 Initial conditions and orbital parameters

We chose the mass of the primary SMBH m_1 to be $4 \times 10^6 M_{\odot}$, and investigated the mass ratio q of the SMBH-SMBH binary in the range $1 - 10^{-4}$ at $[1/2, 1/4, 1/8, \dots, 1/4096]$. The mass of the stars in the stellar binary are both set to be $3M_{\odot}$.

The initial conditions of our restricted four-body problem are then completely defined by ten configuration parameters: three for the SMBH-SMBH binary, three for the orbit of the binary star about the primary SMBH and four for the binary star itself. These are:

- (i) the inclination between the SMBH binary orbit and the binary star orbit, θ ;
- (ii) the longitude of the second black hole's ascending node, l ;
- (iii) the argument of the second black hole's pericenter, ψ ;
- (iv) the semi-major axis of the centre of mass of the stellar binary, a_{CM} ;
- (v) the specific angular momentum of the centre of mass of the stellar binary, j_{CM} ;
- (vi) the mean anomaly of the centre of mass of the stellar binary, M_{CM} ;
- (vii) the inclination of the binary star's inner orbit relative to its center of mass orbit, θ_* ;

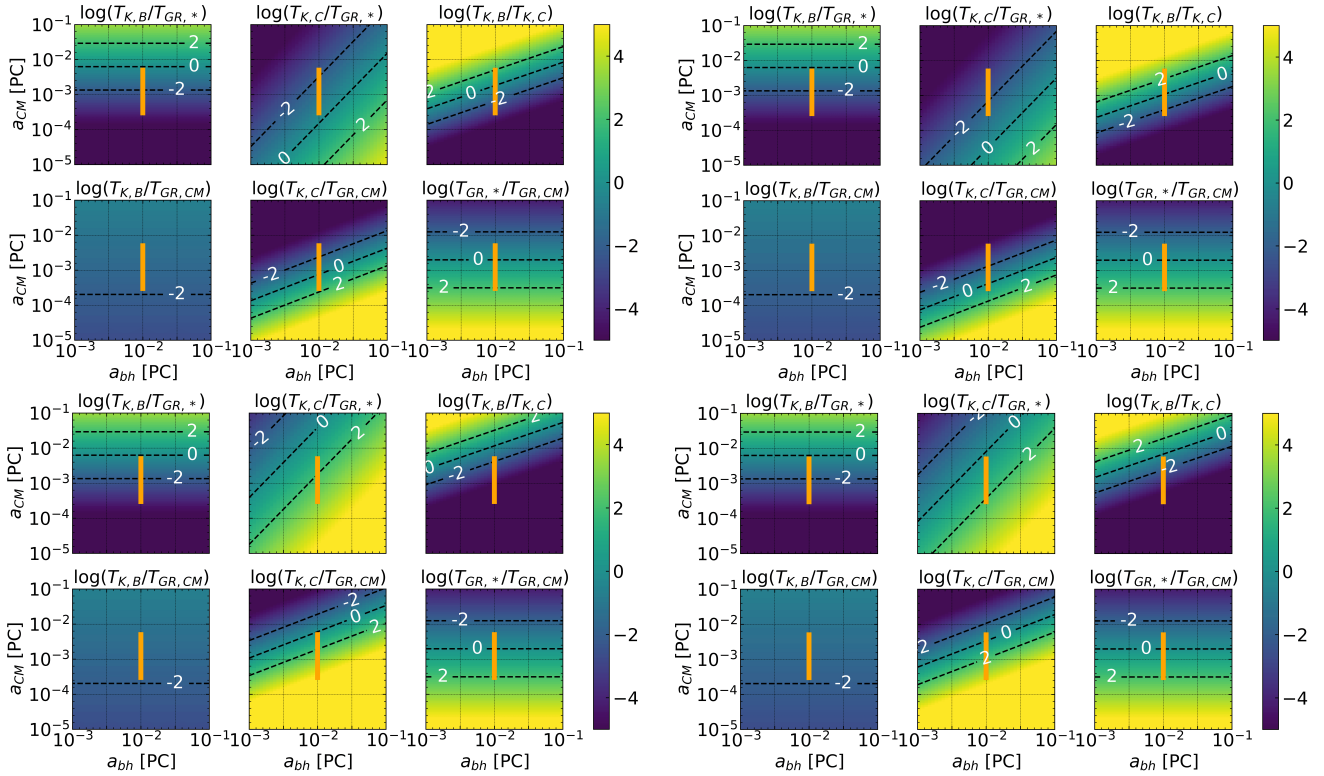


Figure 2. Ratio of different time-scales in our four body system with different values of the eccentricity and mass ratio of the binary SMBH. Here $T_{K,B}$, $T_{K,C}$, $T_{GR,*}$ and $T_{GR,CM}$ correspond to the time scales for, respectively, the inner LK effect, the outer LK effect, general relativistic precession of the stellar binary star and general relativistic precession of the stellar binary centre of mass. The horizontal axis shows the semi-major axis of the SMBH binary. The vertical axis represents the distance between the stellar binary centre of mass and the SMBH. The axes are plotted in log scale, and the colour bar shows the ratio of time scales. The orange lines indicate the parameter space explored in our simulations.

(viii) the longitude of the stars' ascending node in the stellar binary, l_* ;

(ix) the argument of the stars' pericentre in the stellar binary, ψ_* ;

(x) the mean anomaly of the stellar binary, M_* .

For an isotropic stellar distribution, we sample $\cos\theta$ randomly in the range $[-1,1]$, and l, ψ, j_{CM} and M_{CM} randomly in the range $[0,2\pi]$. a_{CM} is sampled randomly in the range $[0.03,0.5]a_{BH}$, while $\cos\theta_*$ is evenly sampled in the range $[-1,1]$. All other phase parameters of the binary star are sampled randomly in the range $[0,2\pi]$. The other two configuration parameters, namely the eccentricity of the stellar binary e_* (set to 0) and the eccentricity of the SMBH binary e_{BH} (set to $[0.3,0.5,0.7]$), are fixed in each group of simulations.

We run 10,000 experiments for each group of input parameters, with an integration end-time of $5(T_{K,B} + T_{K,C})$. In each experiment, particles are deleted from the simulation upon entering either the tidal disruption radius R_{*t} or the event horizon of either SMBH. Similarly, if a particle escapes to a distance $60 a_{BH}$ from the primary SMBH, then the particle is also deleted. A merger event occurs when the distance between two particles becomes less than the sum of their radii. We treat the merger as a completely inelastic collision, hence we delete both particles and create a new particle at the centre of mass. All events - TDEs, mergers and escapes/HVSs - are recorded until either the maximum

integration time is reached or only two particles remain in the system.

4 NUMERICAL EXPLORATION OF THE FOUR-BODY SYSTEM

4.1 Classification of the simulation results

Four types of events are recorded in our four-body simulations. These are TDEs, breakup of stellar binaries, mergers and HVSs. Compound events are made up from these four basic events. For example, two TDEs occurring sequentially within a short time interval make a double TDE. Two HVSs without the breakup of the stellar binary make a double HVS. Binary disruption with a TDE makes a pure single TDE. And so on. In total, there are 11 kinds of compound events.

As shown in Fig.3, we organize the events into a tree structure. At the top root, we perform our simulations with the initial conditions given in Section.3.2. The first level distinguishes between simulations with a binary merger and those without. Once a merger occurs, the four-body system changes into a three-body system. The subsequent evolution of this three-body system, including the formation of TDEs and HVSs, have been well studied. If no merger occurs, a richer set of outcomes are possible relative to the single star case. The additional star makes the second level branch of

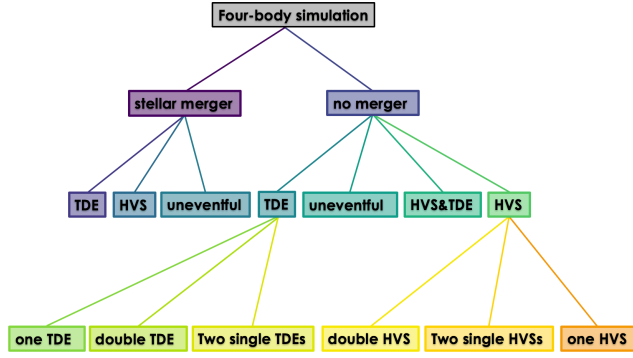


Figure 3. The tree structure of different endings of the encounter of the stellar binaries with the binary SMBH. They are first divided into two groups, with and without mergers. Once a merger occurs, the system becomes a three-body system. The outcomes for this three-body system are a TDE, an HVS or uneventful. If no merger occurs, since there are two stars in the system, an extra event (HVS or TDE) is added to each sub-branch. At the third level of our tree, the TDE and HVS outcomes are both divided into either one TDE (HVS) or two TDEs (HVSs). At the bottom level, we assess the bound status of the binary star as well as the time interval between two successive events. This yields the possible outcomes: a double TDE (HVS), two single TDEs (HVSs), or a TDE and an HVS.

our tree possible. At the second level branch, the outcomes are TDE, HVS, HVS with TDE and uneventful. At the third level, the TDE (HVS) classification is divided into one and two TDEs (HVSs). However, due to the breakup of stellar binary, the two TDE (HVS) case can also be divided into two single TDEs (HVSs) and a double TDE (HVS). The distinction here is the bound status of the stellar binary at the moment of occurrence of the event. The event rates of the branches at a given level or node of the tree always add to unity.

4.1.1 Binary star mergers

Binary star mergers are predominantly caused by orbital eccentricity excitation from LK oscillations in the inner triple system. LK oscillations at the quadrupole level keep the semi-major axis of the orbit a_* constant, such that an increase in the eccentricity leads to a decrease in the pericentre distance $a_*(1 - e_*)$. Once the pericentre is sufficiently small, the two stars collide with each other. The critical distance for this to occur is defined as the sum of the radii of the two stars. Therefore, the merger criterion is

$$a_*(1 - e_*) \leq R_{*,1} + R_{*,2} \quad (15)$$

The stellar radii $R_{*,1}$ and $R_{*,2}$ are calculated from the mass-radius relation $R_* = (m_*/m_\odot)^{0.75} R_\odot$ (e.g., Hansen, Kawaler, & Trimble 2004). The initial a_* is set to 0.1AU and the stellar binary has a total mass set equal to $3m_\odot$ in our simulations. Therefore, the critical eccentricity for merger is $e_{\text{merger}} \sim 0.8$.

As we discuss in Sec.2.2, for our chosen initial conditions, the time scale for relativistic precession of the inner binary orbit $T_{GR,*}$ is much longer than $T_{K,B}$. We do not include dissipative tidal forces in our model. Therefore, the

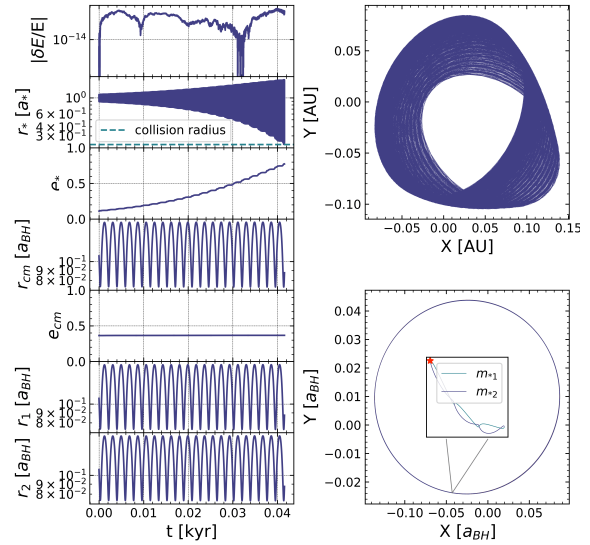


Figure 4. Case study for the merging of stellar binaries. The insets in the left panel show the total energy fluctuation and orbital parameters as a function of time, for a typical merger event. The upper right panel shows the trajectories of the stellar binary components, and the bottom right panel shows the trajectory of the stellar binary centre of mass. The initial conditions are $a_{\text{BH}} = 0.01\text{pc}$, $e_{\text{BH}} = 0.3$, $q = 1/32$, $a_* = 0.1\text{AU}$, $e_* = 0$, $e_{\text{CM}} = 0.3$, $a_{\text{CM}} = 0.12a_{\text{BH}}$, with the inclinations of the inner and outer orbital planes being $i_{\text{in}} = 42.5^\circ$ and $i_{\text{out}} = 1.4^\circ$, respectively.

two main mechanisms for suppressing the LK oscillations and reducing dramatically the orbital separation in the case of mergers (Prodan, Antonini, & Perets 2015) cannot operate. Figure 4 shows an illustrative example of a merger in our simulations. In this example, the inner inclination i_{in} is larger than the critical angle i_c required for LK oscillations, such that the inner LK oscillations excite the eccentricity of the stellar binary orbit e_* until r_* reaches the critical collision distance. The outer inclination i_{out} is smaller than the critical angle, such that the outer LK oscillations are completely suppressed. Therefore, e_{CM} stays the same through the simulation. It is clear in this example that the outer LK oscillations are totally suppressed by the inner LK oscillations. The outer LK oscillations can be absolutely suppressed if $T_{K,B} \ll T_{K,C}$, or by the initial orbital inclination of the outer triple falling out of the range $[i_c, \pi - i_c]$, where $i_c \sim 40^\circ$. From Eqs.6,7 and Fig.2, we speculate that most merger events occur in the inner region (small initial a_{CM}) around the SMBH where $T_{K,B}$ is dominant. For those merger events that occur in the outer region (i.e., with large initial a_{CM}) where $T_{K,B} > T_{K,C}$, the outer LK oscillations are stifled by the small inclination i_{out} . In this way, the inner LK oscillations dominate and finally lead to a stellar merger on a longer timescale compared to at smaller initial a_{CM} .

4.1.2 Tidal Disruption

Tidal disruption is caused by orbital eccentricity excitation in the outer triple system. The perturbation from the secondary SMBH causes the binary star to migrate in closer to the SMBH. Once the binary star reaches the stellar tidal dis-

ruption radius r_{*t} , a TDE occurs. However, due to chaotic perturbations to the binary star, the condition for a stable triple system in Eq. 4 is not upheld in all regions around the primary SMBH. In the region where the triple system remains stable, outer LK oscillations play a fundamental role in exciting the orbital eccentricity. Outside the stable zone, other chaotic dynamical effects can also excite the orbital eccentricity.

If the stellar binary resides in the stable three-body region, LK oscillations become the main mechanism for producing TDEs. From Eq.1, the condition for a TDE is,

$$a_{CM}(1 - e_{CM}) \leq r_{*t} \quad (16)$$

For an SMBH mass $4 \times 10^6 m_{\odot}$, r_{*t} for a $3m_{\odot}$ star is $\sim 1.6\text{AU} = 8 \times 10^{-6}\text{pc}$. In our simulations, the semi-major axis of the SMBH binary is 0.01pc , and the centre of mass of the binary star is sampled evenly between $[0.03, 0.5]a_{BH}$. This yields the typical eccentricity for a TDE $e_{TDE} \sim [0.99, 0.999]$.

Figure 5 shows an illustrative example of a TDE from LK oscillations. In this example, the outer inclination i_{out} is larger than the critical angle, such that the outer LK oscillations excite the eccentricity of the binary star's centre of mass e_{CM} . The inner inclination i_{in} is smaller than the critical angle for LK oscillations i_c , such that the inner LK oscillations are totally suppressed. The binary star maintains a perfectly circular orbit with constant $e_* \sim 0$ until around 0.41kyr , at which point the stellar binary is disrupted due to the tidal force exerted by the primary SMBH m_1 . After this decoupling, the two stars remain in orbit about the primary SMBH. The outer LK oscillations continue to excite the stars' orbits until a single TDE occurs. Unlike for binary mergers, the inner LK oscillations need to be suppressed by the outer LK oscillations in order for a TDE to be produced. The inner LK oscillations can be suppressed either if $T_{K,B} \gg T_{K,C}$, or if the initial orbital inclination of the inner triple falls outside of the range for LK oscillations $[i_c, \pi - i_c]$. From Eqs.6,7 and Fig.2, we conclude that $T_{K,C}/T_{K,B}$ is always smaller in the outer region around the SMBH. Therefore, for binary stars with initial semi-major axis a_{CM} in this area, TDEs occur more frequently than HVSs. TDE events can also occur in the inner region around the SMBH, but only if the binary's orbit is nearly coplanar with the orbit of the binary centre of mass about the SMBH. In this case, the inner LK oscillations that drive stellar mergers cannot be activated due to the low inclination i_{in} . The maximum eccentricity that can be induced by LK oscillations is constrained by the initial inclination $e_{max} = \sqrt{1 - \frac{5}{3} \cos^2 i_{int}}$. The high eccentricity needed for TDEs ($[0.99, 0.999]$) requires that the orbital plane of the binary centre of mass about the SMBH be nearly perpendicular to the binary's orbital plane.

If Eq. 4 is not satisfied, the system becomes chaotic. Chaotic effects could also excite the eccentricity (e.g., Chen et al. 2009). Unlike quadrupole LK oscillations, chaotic effects do not conserve the semi-major axis of the orbit. Consequently, the subsequent evolution can be difficult to predict. However, the simulation results allow us to study chaotic excitations statistically.

Figure 6 shows an illustrative example of chaotic excitations. The stellar binary maintains an almost elliptical orbit at the beginning of the simulation. The first close encounter

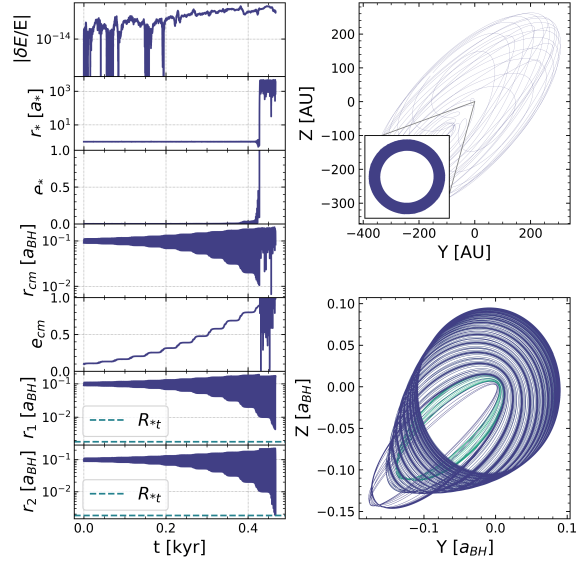


Figure 5. Case study for TDE. Same as Fig. 4, but the adopted initial condition is different, namely $a_{BH} = 0.01\text{pc}$, $e_{BH} = 0.5$, $q = 1/2$, $a_* = 0.1\text{AU}$, $e_* = 0$, $e_{CM} = 0.1$, $a_{CM} = 0.1a_{BH}$, with the inclination of the inner and outer orbits being $i_{in} = 24.2^\circ$ and $i_{out} = 89.9^\circ$, respectively. The stellar binary centre of mass remains in a circular orbit until the binary is disrupted.

with the SMBH, which occurs around 0.08kyr , causes the stellar binary to become more compact. At the same time, the eccentricity of the centre of mass of the stellar binary's orbit about the SMBH is suddenly excited. This excitation leads to an extremely high eccentricity, which subsequently produces a double TDE during the second close encounter.

4.1.3 Hypervelocity Stars

Hypervelocity stars can be produced by the slingshot effect (Lu, Yu, & Lin 2007), or the interaction between a globular cluster and an SMBH/SMBHB (Capuzzo-Dolcetta & Fragione 2015; Fragione & Capuzzo-Dolcetta 2016; Fragione, Capuzzo-Dolcetta, & Kroupa 2017). In our simulations, most binary stars remain within the Hill sphere of the primary SMBH. In a stable hierarchical triple system, LK oscillations cannot produce HVSs because they conserve the semi-major axis of the orbit. However, if we replace the single star in a triple system with a stellar binary, the binary can be disrupted at the tidal breakup radius of the stellar binary r_{bt} , which re-distributes energy and angular momentum within the four-body system. This energy and angular momentum re-allocation can produce HVSs.

Figure 7 shows an illustrative example of a double HVS. The inner i_{in} inclination is smaller than the critical angle, such that the inner LK oscillations are suppressed. The outer i_{out} inclination is larger than the critical angle. Therefore, the outer LK oscillations should result in an excitation of the orbit of the centre of mass of the stellar binary. However, since $a_{CM} = 0.34a_{BH}$, $q = 1/2$ and $e_{BH} = 0.9$, the secondary SMBH gets very close to the stellar binary, leading instead to an ejection event. The distance to the SMBH of the stellar binary is insufficiently small for it to be disrupted after a slight oscillation, and a double HVS occurs instead. Most HVSs are the result of a strong perturbation from the

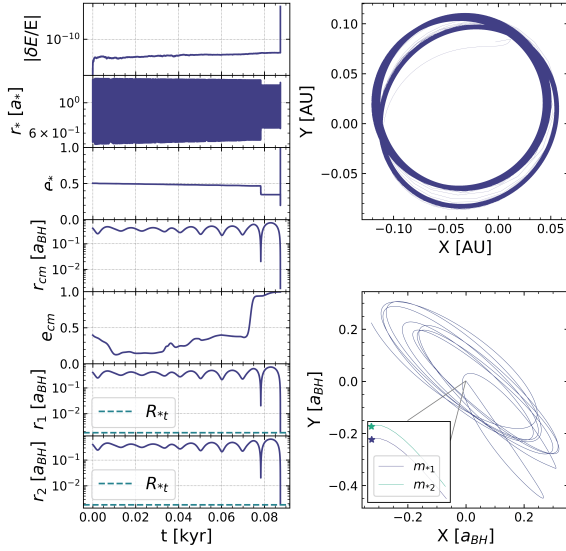


Figure 6. Case study for double TDE. The initial conditions for a typical double TDE are $a_{\text{BH}} = 0.01\text{pc}$, $e_{\text{BH}} = 0.3$, $q = 1/32$, $a_* = 0.1\text{AU}$, $e_* = 0$, $e_{\text{CM}} = 0.45$, $a_{\text{CM}} = 0.5a_{\text{BH}}$, with the inclination of the inner and outer orbits being $i_{\text{in}} = 5.2^\circ$ $i_{\text{out}} = 8.6^\circ$, respectively. The outer i_{out} and inner i_{in} inclinations are both smaller than the critical angle, such that both the inner and outer LK oscillations are suppressed. However, since $a_{\text{CM}} = 0.5a_{\text{BH}}$, the system is no longer a stable hierarchical triple system, and chaotic effects excite the eccentricity e_{CM} in an irregular way.

secondary SMBH, which occurs most frequently for larger mass ratios q and higher eccentricities e_{BH} . Such a strong perturbation can even result in a double HVS event.

4.2 Event rates for different SMBH binary mass ratios

LK oscillations in the inner and outer triple, together with non-secular effects and chaotic effects, influence the orbital evolution of the main sequence binary. The efficiency of the inner and outer LK oscillations depends on the relative ratio of their respective time scales. As Eq. 6 and 7 shown, the relative time scales of the inner and outer LK oscillations are sensitive to the ratios a_{CM}/a_* and $a_{\text{BH}}/a_{\text{CM}}$. In our simulations, we fix the semi major axis of the stellar binary to reduce the free parameters in our model. Regardless, how a_* affects the outcome is readily apparent from our simulations. When the inner LK oscillations dominate, the fraction of stellar mergers becomes large (as shown in Fig.11). In this case, the choice of binary mass and semi-major axis will affect the merger rate significantly. If the semi-major axis of the SMBH-SMBH binary and that of the stellar binary's orbit about the primary SMBH are fixed, compact stellar binaries are harder to merger. This is because smaller values for a_* yield longer time scales for the inner LK oscillations to operate. On the other hand, when the outer LK oscillations dominate, the choice of binary mass and semi-major axis do not influence the TDE and HVS event rates significantly. Here, the stellar binary can effectively be regarded as a single particle.

The presence of a background gravitational potential could also affect the relative event rates. In particular, in

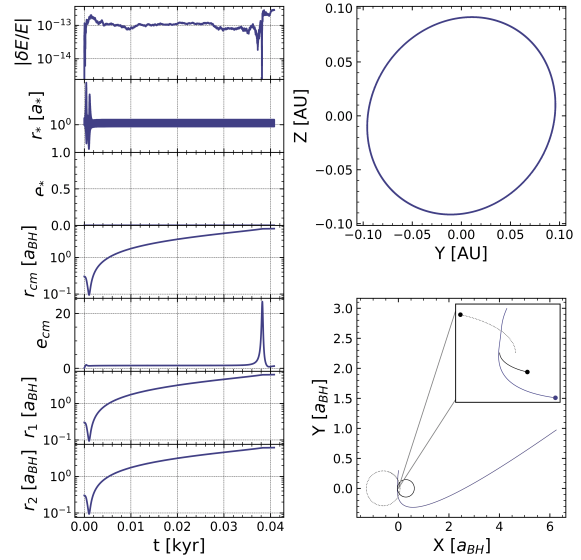


Figure 7. Case study for double HVSs. The initial conditions for a typical double HVS are $a_{\text{BH}} = 0.01\text{pc}$, $e_{\text{BH}} = 0.9$, $q = 1/2$, $a_* = 0.1\text{AU}$, $e_* = 0$, $e_{\text{CM}} = 0.11$, $a_{\text{CM}} = 0.34a_{\text{BH}}$, with the inclination of the inner and outer orbits being $i_{\text{in}} = 1.4^\circ$ $i_{\text{out}} = 67.3^\circ$, respectively. After the ejection, the stellar binary recedes from the SMBH binary system. Consequently, the eccentricity e_{BH} , which is defined as the orbital eccentricity around the primary SMBH m_1 , diverges to infinity.

the Galactic Centre, dim low-mass stars are not detectable, and it is not known if any contribute to the local potential in the immediate vicinity of the primary SMBH. Any contribution to the potential from gas and/or dust is also not included in our calculations. Naively, however, we expect these contributions to have a negligible effect on the results reported in this paper. Scattering experiments under the presence of a background potential were recently performed by (Ryu, Leigh, & Perna 2017), and subsequently applied to the production of runaway and hypervelocity stars (Ryu, Leigh, & Perna 2017). It was shown that, unless the potential is very deep, the outcome of the scattering experiment is not significantly affected.

To quantify the significance of the secondary SMBH in deciding each outcome, we vary the mass ratio of the SMBH binary. Figure 8 depicts the rates of different events as a function of the mass ratio q , for different eccentricities e_{BH} .

As the mass ratio increases, so do the total event rates. This is especially true for the double HVS rates. The TDE rates form a peak between $q = 10^{-2}$ and $q = 10^{-1}$. The 'star' at the left end of each curve shows the event rates for a single SMBH ($q = 0$) obtained from three-body simulations. The event rates for the SMBH-SMBH binary converge to the single SMBH case when $q \rightarrow 0$, except for single TDEs and single HVSs. The single TDEs (HVSs) come from the decoupling of the stellar binary, which is sensitive to the mass of the secondary SMBH. For the mass ratio $1/4096$, the mass of the secondary SMBH is still not small enough to neglect the effect on decoupling due to the secondary SMBH. Overall, the event rates for an SMBH-SMBH binary are always different than those obtained for a single SMBH. Consequently, the observed relative event rates can be used to constrain the possible presence of a binary SMBH companion orbiting

the central primary SMBH in the Galactic Centre. We will return to this interesting possibility in Section 5.

Figure 9 shows the relative rates for the different events shown in Fig. 3 for $e_{\text{BH}} = 0.5$. Both the TDE and HVS rates increase with increasing mass ratio q .

4.2.1 Merger Rate as a function of Mass Ratio

The most common event in our four-body system is stellar mergers. The merger events correspond to initial conditions for which the inner LK oscillations dominate. Fig. 10 shows the fraction of merger events arising from different effects. We see that most merger events are due to LK oscillations. Therefore, the efficiency of the LK oscillations is what decides the dependence of the total merger rate on mass ratio q . The upper panel of Fig. 11 shows the merger rates for different mass ratio. This mechanism should be independent of the mass of the second SMBH $m_2(q)$, since it is driven by the inner LK oscillations coming from the primary SMBH. However, the upper panel of Fig. 11 indicates that the merger rate increases slightly with increasing mass ratio. The reason for this slight increase is that the inner and outer LK oscillations are not completely independent. In regions where both the inner and outer LK oscillations affect the stellar binary, the outer LK oscillations could excite the stellar binary to migrate in closer to the primary SMBH m_1 , where the inner LK oscillations are stronger, leading to higher merger rates. The peak of the merger rate appears between $q \sim 10^{-2}$ and $q \sim 10^{-1}$. Above the peak mass ratio, the merger rate starts to decrease due to the four-body system more frequently becoming unstable. Larger masses for the secondary SMBH m_2 weaken both the inner and outer LK oscillations. Consequently, in this case, the merger rate decreases with increasing mass ratio. At the far left end, all lines converge to the star, which represents the merger rate for the single SMBH case.

The lower panel of Fig. 11 shows the relative probabilities for the occurrence of stellar mergers. The initial parameters considered in each of the four insets are (a_{CM}, q) , (e_{CM}, q) , (i_{in}, q) and (i_{out}, q) . The colours quantify the relative probabilities in these parameter spaces. The first inset shows that mergers are more likely to occur at small a_{CM} and large q . This is because, from Eq. 6 and Eq. 7, smaller a_{CM} and larger q translates in to stronger inner LK oscillations compared to the outer LK oscillations. The third inset shows that most mergers happen when the inclination i_{in} nears 90° . This region is ideal for LK oscillations to operate effectively. The last inset confirms our earlier hypothesis, in the upper panel of Fig. 11, namely that the outer LK oscillations also contribute to mergers when i_{out} even weakly concentrates at high inclination.

4.2.2 HVS rate enhancement

An interesting effect seen in our four-body system is a rapid increase in the HVS rate with increasing mass ratio. The upper panel of Fig. 12 shows the total HVS rates for different mass ratios q and eccentricities e_{BH} . For very small mass ratios, the lines converge to the single SMBH case, and the HVS rate is nearly zero. Near the lowest mass ratios $q \sim 10^{-2}$, the stability of the four-body system might be

affected and breakup is possible. At larger mass ratios, the HVS rate increases significantly with increasing mass ratio q . This can potentially be explained by the strong perturbation induced from the secondary SMBH m_2 on the stellar binary, which could transfer energy and angular momentum to the binary. This could even result in the collisional ejection of the binary. The bottom right panel of Fig. 7 shows a good example of this process. As is clear, a larger secondary SMBH mass m_2 along with a closer distance from the primary SMBH (i.e., larger e_{BH}) result in stronger perturbations, which translates in to an elevated rate of HVS production.

The lower panel of Fig. 12 shows that HVSs are more likely to be produced at larger a_{CM} . This is because binaries at smaller a_{CM} are more likely to be consumed as TDEs due to LK oscillations. This panel also indicates that the HVS rate is independent of the outer inclination i_{out} , but increases near the critical angle for LK oscillations, namely $i_c \sim 40^\circ$ and 140° for i_{out} .

Figure 13 shows the HVS velocity distribution measured at the escape distance, or $60 a_{\text{BH}}$ from the centre of mass of the SMBH binary. The typical escape velocity is $\sim 300 - 1000 \text{ km s}^{-1}$, which fits the observations very well.

4.2.3 TDE rate enhancement

Fig. 14 shows the fraction of TDEs driven by secular versus non-secular effects. We see that the relative fractions are sensitive to the eccentricity of the SMBH binary. With increasing e_{BH} , non-secular and chaotic effects become significant. The relative fraction has only a weak dependence on the mass ratio of the SMBH binary. However, the total TDE rate is enhanced significantly due to the presence of the secondary SMBH. LK oscillations driven by the outer orbit are the main source of the increase in the TDE rate. Equation 7 shows the outer LK oscillation time-scale $\sim (1 - e_{\text{BH}}^2)^{3/2}/q$. Both the mass ratio q and the eccentricity e_{BH} increase quickly, along with a decrease in the time-scale for LK oscillations, leading to enhanced orbital excitation in the outer triple. This explains the observed increase in the TDE rate for $q \lesssim 10^{-2}$ (see the upper panel of Fig. 15). As the mass ratio q increases, the stellar binary begins to feel the effects of the increasingly massive secondary SMBH m_2 . Consequently, the LK oscillations in the outer triple are gradually reduced by the presence of the secondary SMBH m_2 . This is the reason for finding that the TDE rate does not increase and can even decrease at larger mass ratios. The TDE rate for the single SMBH case at the far left end drops from $\sim 3\%$ to $\sim 1.5\%$. This is due to the gap in the single TDE rate from Fig. 8.

The second SMBH m_2 enhances the TDE rate significantly, from 2.8% to 17.6% for $e_{\text{BH}} = 0.3$ and from 2.8% to 30.8% for $e_{\text{BH}} = 0.9$. The LK oscillations require that the outer triple orbit must have an outer inclination $40^\circ < i_{\text{out}} < 140^\circ$. The lower panel of Fig. 15 shows these effects mediated by LK oscillations. Most TDEs appear at high inclinations i_{out} , when the outer LK oscillations dominate. This panel also clearly illustrates that the TDE rate is independent of the inner inclination i_{in} .

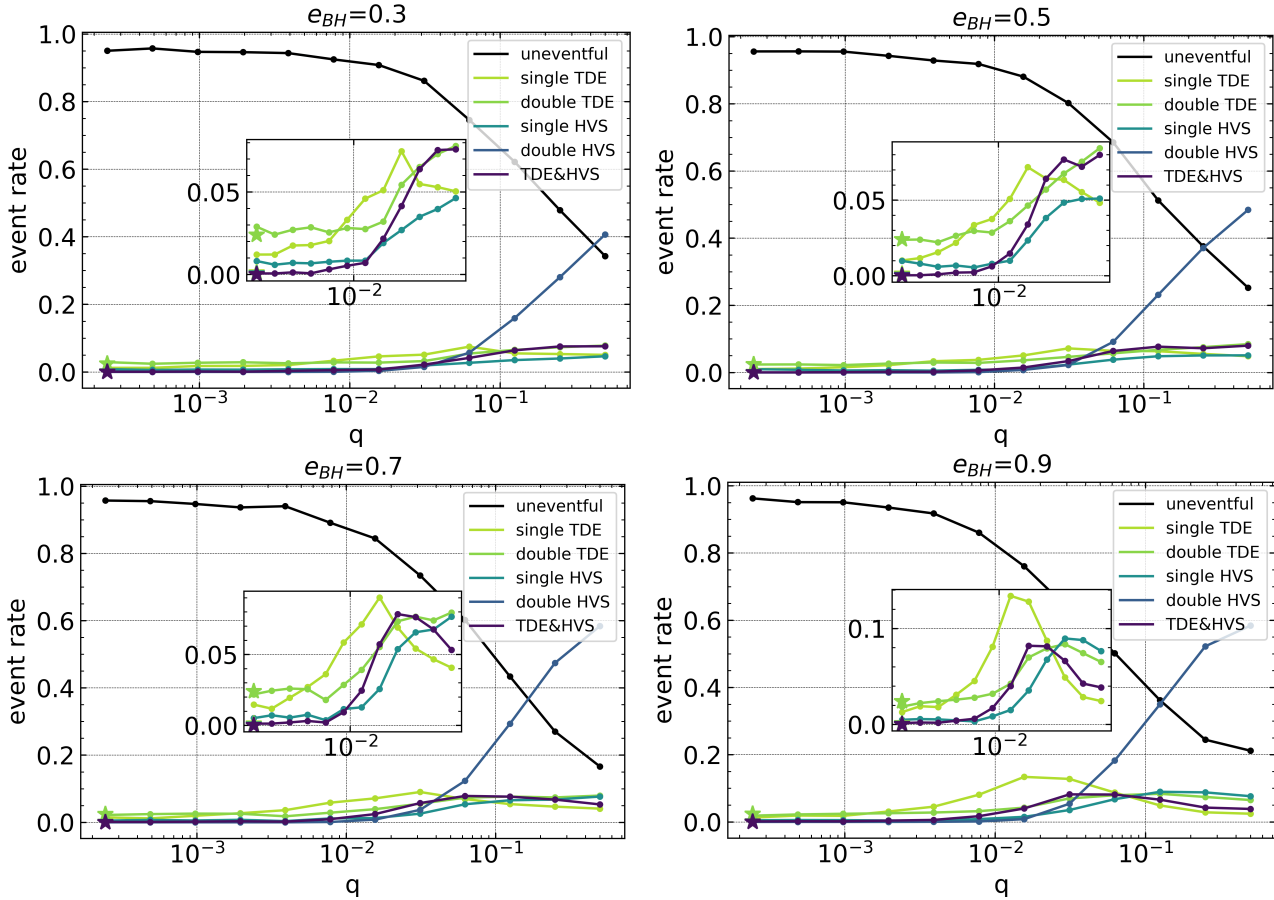


Figure 8. Event rates as a function of mass ratio of binary SMBH. All events are shown in Fig. 3. These events are: uneventful, single TDE, double TDE, single HVS, double HVS and TDE with HVS. The HVS rates continually increase after the activation threshold near $q \sim 10^{-2}$. Larger eccentricities e_{BH} accelerate the rate of increase, due to stronger perturbations at pericentre. The maximum TDE rates occur between $q \sim 10^{-2}$ and $q \sim 10^{-1}$.

4.2.4 HVS with TDE

A special event in this four-body system is the simultaneous occurrence of an HVS with a TDE. The stellar binary is disrupted when r_* reaches the Hill radius r_{Hill} . One of the stars then gets ejected as an HVS, while the other star falls into the tidal radius r_{t*} of one of the SMBHs (usually the primary, but see Figure 17). The binary disruption plays a fundamental role in this special event. As discussed in Section 4.2.2, in certain regions of the relevant parameter space, the secondary SMBH can transfer energy and angular momentum to the stellar binary. Subsequently, the binary can be collisionally ejected from the system. If the distance of the stellar binary to the primary SMBH m_1 remains sufficiently large, the stellar binary can remain bound and be ejected as a bound object.

Figure 16 shows the event rate for the simultaneous formation of an HVS and a TDE (i.e., HVS&TDE combination), for different eccentricities e_{CM} . The simulated data resemble what we would naively expect from a simple superposition of the TDE and HVS data, albeit with a few additional modifications. Although the dependence of energy and angular momentum redistribution within the four-body system on the mass ratio q is not completely understood, we can still draw reliable conclusions from the lower panel

of Fig. 16. In mass ratio-space, the HVS&TDE combination looks very similar to what is seen for the TDE case alone, with the exception that the former outcome extends out beyond this region to the upper right. The inner inclination i_{in} concentrates at low inclination angles, such that no binary merger events occur. The outer inclination i_{out} concentrates at high inclination angles, such that the decoupled star can be excited in to the tidal disruption radius.

4.3 TDE from the Secondary SMBH

Both the Schwarzschild radius R_s and the tidal disruption radius for stars r_{*t} increase with increasing SMBH mass. The tidal disruption radius r_{*t} is given by Eq. 1, and the Schwarzschild radius is

$$R_s = \frac{2Gm_{BH}}{c^2}. \quad (17)$$

Above a critical BH mass $m_{BH,crit}$, the Schwarzschild radius becomes greater than the tidal disruption radius. Above this critical SMBH mass it should not be possible to observe any TDEs, because the SMBH will swallow the whole stars and no light will escape from within R_s . In the limit of a primary SMBH with mass $m_1 > m_{BH,crit}$, but a secondary with mass $m_2 < m_{BH,crit}$, it is only the secondary SMBH that can

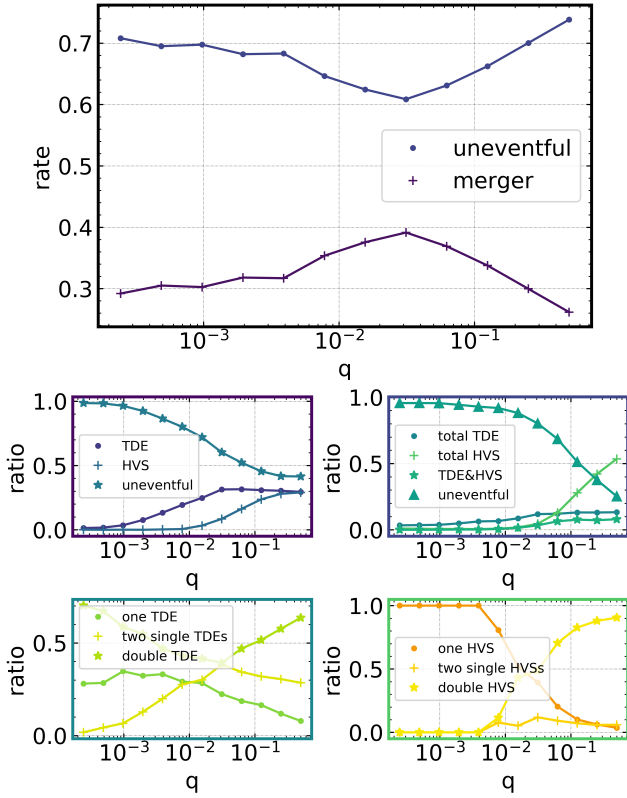


Figure 9. The relative rates of events as shown in Fig. 3. The top inset shows the rates for the upper branches of the tree in Fig. 3. The middle panel shows the middle branches, and the bottom panel shows the lower branches. The color of each event box in Fig. 3 is identical to the corresponding event colour here.

cause TDE events. By incorporating the empirical $M_{\text{BH}} - M_{\text{gal}}$ relation (e.g Kormendy & Ho 2013; Georgiev et al. 2016), this opens up the possibility to use TDEs as detectors for secondary SMBHs/IMBHs orbiting in the nucleus of a far away galaxy. This is because, since the $M_{\text{BH}} - M_{\text{g}}$ relation increases monotonically, it can be used to convert the critical BH mass $m_{\text{BH,crit}}$ into a critical galaxy mass $M_{\text{g,crit}}$, above which no TDEs should be produced by the central SMBH. However, this assumes that the central massive BH in every galaxy is isolated. Cosmological simulations, on the other hand, suggest that both major and minor mergers between galaxy pairs occur frequently, and in the process deliver their own central SMBHs to the nuclear regions of the product of this galaxy-galaxy merger. This could predict the presence of a large population of secondary SMBHs in galaxies, in presumably stable orbits about the primary SMBH.

The presence of the secondary SMBH in orbit around the primary SMBH opens the door to observing TDEs from the secondary SMBH. But we do not know how often this should occur, if ever. To answer this question, Figure 17 shows the relative probability for a secondary-induced TDE for different mass ratios q and different eccentricities e_{BH} . As is clear, the secondary always contributes to the total rate of TDEs, but only by a few percent at very low mass ratios. At larger mass ratios, the fraction of TDEs produced by the secondary increases steadily, converging toward 50% at $q = 1$. Importantly, independent of the mass ratio, the secondary

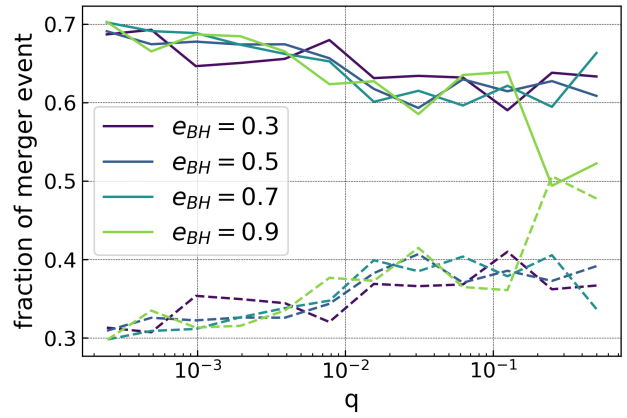


Figure 10. The fraction of the event rate of stellar merging due to the secular effects versus non-secular or chaotic effects for different eccentricities of the SMBH binary. The solid lines show the fraction of the event rate of stellar merging driven by the inner LK oscillations. The dashed lines show the fraction of the event rate of stellar merging due to the non-secular or chaotic effects.

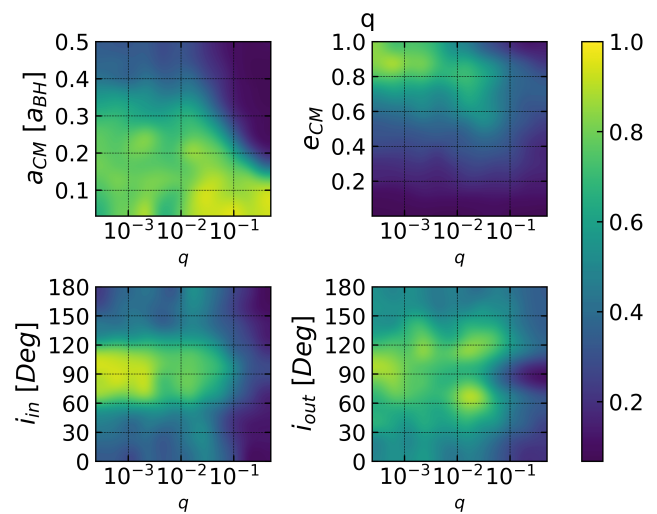
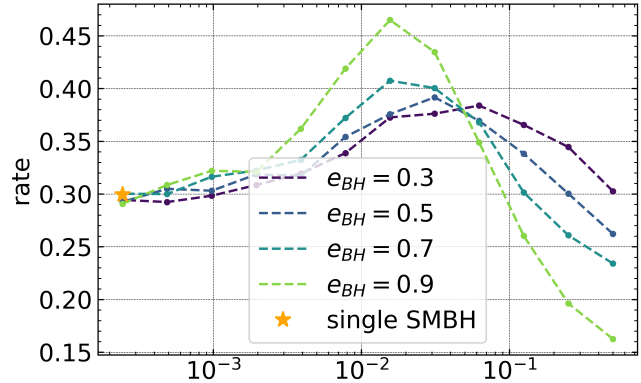


Figure 11. Rates of mergers of stellar binaries. The upper panel shows the merger rates for different mass ratios q . The merger rate increases with increasing mass ratio q , at least until m_2 becomes too massive and breaks the hierarchical structure of the four-body system. The colours in the bottom panel quantify the relative merger probability in the indicated parameter space.

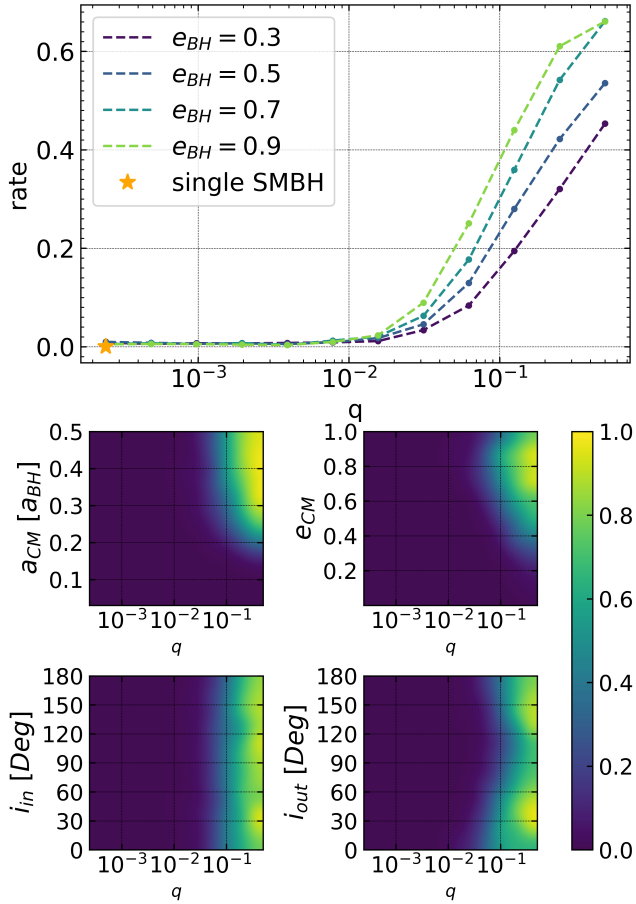


Figure 12. Event rates of HVS versus the mass ratio of binary SMBH with different e_{BH} . The upper panel shows that HVSs begin to be produced at $q \sim 10^{-2}$, and the rate increases at larger mass ratios. The lower panel shows the HVS rates in colour-space. The yellow regions indicate the highest HVS rates and appear at large q , large a_{CM} , large e_{CM} and near the critical angle for LK oscillations to occur, $i_c \sim 40^\circ$ or 140° .

always contributes a base minimum of a few percent to the total TDE rate. Extrapolating this result to even lower mass ratios suggests that even stellar-mass BHs closely orbiting a central SMBH have a non-negligible probability of causing a TDE. This begs the question: If ~ 100 stellar-mass BHs are in close orbits about a central massive SMBH, and each one should contribute of order a percent to the total observed TDE rate, then does the TDE rate from the SMBH become nearly equal to the TDE rate from the swarm of stellar-mass BHs? We intend to explore this interesting question in more detail in future work.

5 SUMMARY

In this work, we have studied the fate of main sequence stellar binaries orbiting around a primary central SMBH perturbed by a remote secondary SMBH, as a function of the mass ratio of SMBH-SMBH binaries. The presence of the secondary SMBH significantly changes the evolution of these stellar binaries, and the relative rates of observable astrophysical phenomena. We have performed N -body simula-

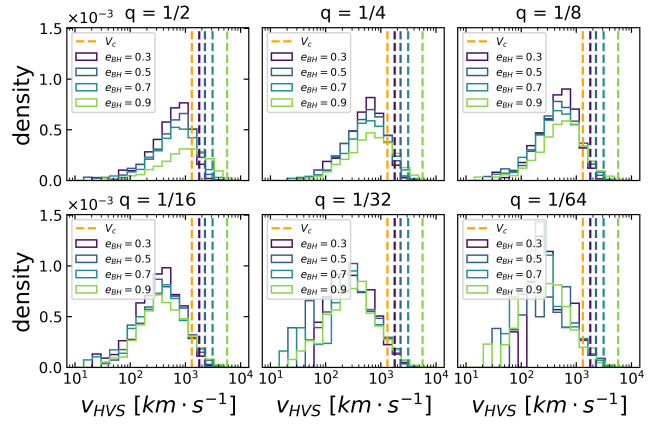


Figure 13. Distribution of the normalized HVS velocity at escape radius $60 a_{BH}$ from the centre of mass of the SMBH binary, for different mass ratios q and eccentricities e_{BH} of the binary SMBH. Here $V_c = \sqrt{Gm_1/a_{BH}}$ is the binary orbital velocity of the SMBH binary. The dashed lines show, for each binary model with a given eccentricity, the velocity of the secondary SMBH at the pericenter.

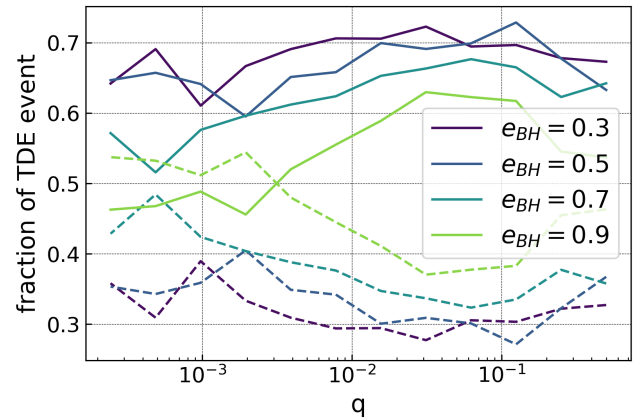


Figure 14. The fraction of TDEs due to the secular effects versus the non-secular or chaotic effects as a function of the mass ratio of the SMBH binary for different eccentricities of the SMBH binary. The solid lines show the fraction of TDEs driven by the outer LK oscillations. The dashed lines show the fraction of TDEs due to the non-secular or chaotic effects.

tions of this four-body system with different SMBH-SMBH binary mass ratios, and analyzed the fate of the system. Our main conclusions can be summarized as follows.

Our simulations show that the total event (TDE, HVS, merger) rates are increased by the presence of a secondary SMBH m_2 , and continue to increase as m_2 increases (Figure 8 indicates that the fraction of uneventful simulations continuously decreases as the mass ratio increases). The presence of the secondary SMBH acts to migrate the stars toward the primary SMBH via the outer LK oscillations, where they are consumed by TDEs, HVSs and mergers. This suggests that galaxies observed to exhibit higher rates of extreme astrophysical events (i.e., TDEs, HVSs, mergers) are more likely to harbour an SMBH binary.

Merger events mainly occur due to the inner LK oscillations. Equation 6 shows the timescale for the inner LK os-

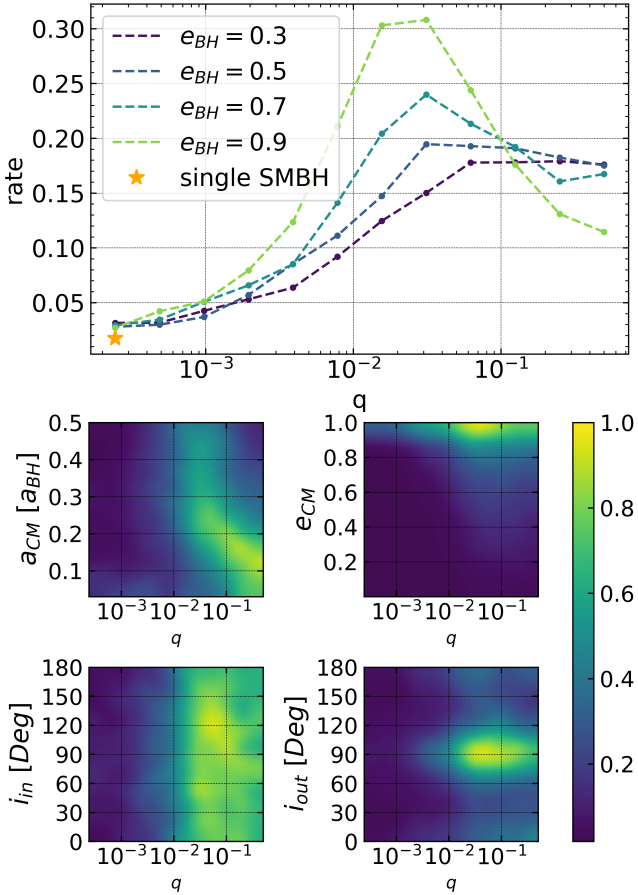


Figure 15. TDE rates versus mass ratio of the binary SMBH with different e_{BH} . The upper panel illustrates a significant enhancement in the TDE rates at larger mass ratios q , at least up to ~ 0.03 . Chaotic effects are responsible for the TDE rate decrease at larger values of q . The lower panel illustrates the primary effect we have attributed to the outer LK oscillations - TDE rates are high at high inclination i_{out} for the outer orbit, and independent of the inner inclination i_{in} . The first inset, which plots $a_{CM} - q$, shows the stability boundary for hierarchical triples.

oscillations to operate. For a given stellar mass density profile (i.e., given a distribution in a_{CM}), the merger rate in a galaxy is determined by the properties of its primary SMBH. However, our simulations show that the secondary SMBH could slightly increase the merger rate in the range $q \sim < 10^{-2}$. In this mass ratio range, the secondary SMBH transports more stars to the inner regions near the primary SMBH. Here, the inner LK oscillations are stronger, leading to higher merger rates.

HVSs are produced from the decoupling of the stellar binary at its break up radius r_{bt} due to the primary SMBH. Previous work indicates that this decoupling tends to produce HVSs by ejecting one of the stars in the binary. Our simulations show that the rate for this process to operate is very low (see the rates of single HVSs in Figure 8). In this work, we have identified a more efficient way to produce HVSs, namely via strong perturbations from the secondary SMBH. These strong perturbations can even eject the stellar binary at pericenter without unbinding the binary. The rate for this process increases rapidly above mass ratios

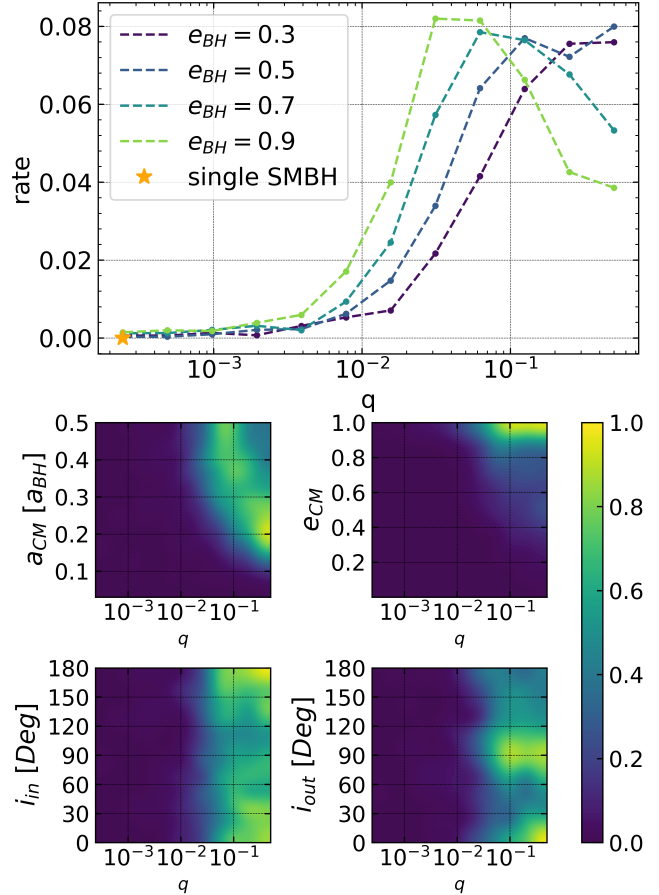


Figure 16. The rates for the simultaneous production of an HVS and a TDE as a function of the mass ratio of the binary SMBH with different e_{BH} . The upper panel shows the presence, albeit with low probability, of this special event in our four-body system. The bottom panel shows the relative probability for the occurrence of this event in each parameter space. The TDE&HVS combination tends to occur at high inclination angles for the outer orbit i_{out} and low inclination angles for the inner orbit i_{in} .

$q \geq 10^{-2}$ (see Figure 12). These ‘double HVSs’ should only be produced by SMBH binaries, with a rate much higher than for single HVSs.¹ Hence, hypervelocity binary star systems could be regarded as a smoking gun for the presence of an SMBH binary (Lu, Yu, & Lin 2007; Sesana, Madau, & Haardt 2009). Incidentally, one such system has possibly been identified in the Milky Way (Brown et al. 2010). Figure 13 shows the HVS velocity distribution evaluated at a distance of $60 a_{BH}$ from the SMBH primary. The typical velocities range from 300 km s^{-1} to 1000 km s^{-1} , depending on the mass ratio of the SMBH-SMBH binary. To compare the distribution of HVS velocities with observations more precisely, the Galactic potential must be taken into consideration, which will be done in a follow up paper (Wang et al. in prep.). In turn, the Galactic potential can be constrained from the observed distribution of HVSs using the upcoming

¹ Note that this does not account for direct interactions between a single SMBH and stellar triple systems (e.g. Perets & Subr 2012), but the rate of these interactions should be very low (Leigh & Geller 2013).

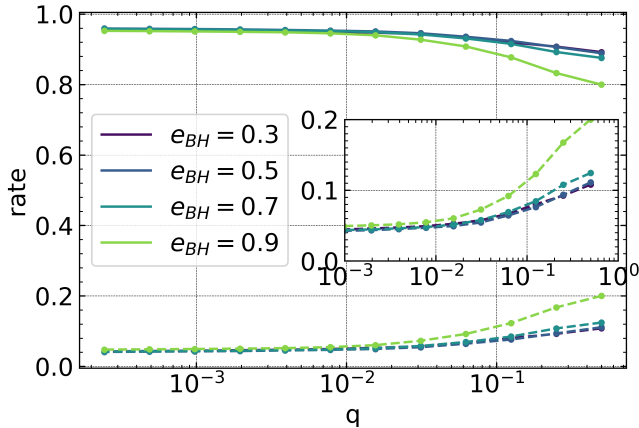


Figure 17. The event rates of TDE by both the primary and the secondary black holes as function of the mass ratio of binary SMBH. The solid lines show the fraction of TDEs occurring around the primary SMBH. The dashed lines show the fraction of TDEs occurring around the secondary SMBH. The curves at different eccentricity all converge to a few percent below $q \sim 10^{-3}$, such that the ratio becomes roughly independent of q . At large mass ratios (i.e., after $q \sim 10^{-2}$), the fraction of TDEs from the secondary SMBH quickly increases.

data from the Gaia satellite, as discussed in (Kenyon et al. 2014; Fragione, Ginsburg, & Kocsis 2017; Marchetti et al. 2017).

The TDE rate is quite low for the single SMBH case, relative to the SMBH-SMBH binary case. This is because the secondary SMBH acts to migrate stars to the inner region around the primary SMBH via strong outer LK oscillations. This effect could focus the stars to the centre of the galaxy, close to the primary SMBH, and in the process accelerate the rate of tidal disruption events. The secondary SMBH increases the TDE rate significantly at large mass ratios q . Therefore, this opens up the possibility of using the relative rates of TDEs and HVSs to observationally constrain the occurrence of SMBH-SMBH binaries in galactic nuclei.

TDEs often occur due to disruption by the secondary SMBH, instead of the primary. This opens up the possibility of observing TDEs in massive galaxies with the most massive central SMBHs, when no TDEs should be expected. This is because, via the M - σ relation, the host SMBH should have a mass above the critical mass for TDEs to occur inside the Schwarzschild radius $R_S > r_{*,t}$. Hence, no TDEs should be produced by the most massive SMBHs in the most massive galaxies. Thus, the observation of even a single TDE in such a massive galaxy would be the smoking gun of a secondary lower mass SMBH companion.

Our results show that the presence of a secondary SMBH changes the relative rates of TDEs and HVSs relative to the isolated SMBH case. Hence, observations of these two phenomena could help to constrain the possible presence of a central IMBH in the Galactic Centre, and/or the presence of SMBH-SMBH binaries in the nuclei of other galaxies. The dependence of the event rates in our simulations on the SMBH-SMBH binary mass ratio could potentially be used to constrain the frequency of SMBH-SMBH binaries in galactic nuclei, and even their mass ratio distribution. To this aim, a follow up paper (Wang et al. in prep.) will be

devoted to a detailed comparison between simulations and all the available observational data.

ACKNOWLEDGMENTS

YFY is supported by National Natural Science Foundation of China (Grant No. U1431228, 11725312, 11233003, and 11421303). Results in this paper were obtained using the high-performance Lired computing system at the Institute for Advanced Computational Science at Stony Brook University, which was obtained through the Empire State Development grant NYS #28451.

REFERENCES

- Alexander T., 2005, PhR, 419, 65
 Anderson K. R., Storch N. I., Lai D., 2016, MNRAS, 456, 3671
 Antonini F., Faber J., Gualandris A., Merritt D., 2010, ApJ, 713, 90
 Antonini F., Murray N., Mikkola S., 2014, ApJ, 781, 45
 Antonini F., Murray N., Mikkola S., 2014, ApJ, 781, 45
 Blaes O., Lee M. H., Socrates A., 2002, ApJ, 578, 775
 Brown W. R., Anderson J., Gnedin O. Y., Bond H. E., Geller M. J., Kenyon S. J., Livio M. 2010, ApJL, 719, L23
 Capuzzo-Dolcetta R., Fragione G., 2015, MNRAS, 454, 2677
 Fragione G., Capuzzo-Dolcetta R., 2016, MNRAS, 458, 2596
 Fragione G., Capuzzo-Dolcetta R., Kroupa P., 2017, MNRAS, 467, 451
 Chen X., Madau P., Sesana A., Liu F. K., 2009, ApJ, 697, L149
 Eggleton P. P. & Kiseleva-Eggleton L., 2001, ApJ, 562, 1012
 Fabrycky D. C., Tremaine S. 2007 ApJ 669 1298
 Fragione G., Loeb A., 2017, NewA, 55, 32
 Fragione G., Ginsburg I., Kocsis B., 2017, arXiv, arXiv:1711.00483
 Georgiev I., Böker T., Leigh N. W. C., Lützgendorf N., Neumayer N. 2016, MNRAS, 457, 2122
 Gezari S., et al., 2012, Nature, 485, 217
 Gillessen S., et al., 2017, ApJ, 837, 30
 Ginsburg I., Loeb A., 2007, MNRAS, 376, 492
 Gualandris A., Portegies Zwart S., Sipior M. S., 2005, MNRAS, 363, 223
 Gualandris A., Merritt D., 2009, ApJ, 705, 361
 Hansen C. J., Kawaler S. D., Trimble V., 2004, sipp.book
 Hills J. G., 1975, Nature, 254, 295
 Hills J. G., 1988, Nature, 331, 687
 Holman M., Touma J., Tremaine S., 1997, Nature, 386, 254
 Innanen K. A., Zheng J. Q., Mikkola S., Valtonen M. J., 1997, AJ, 113, 1915
 Katz B., Dong S., 2012, preprint (arXiv:1211.4584)
 Kenyon S. J., Bromley B. C., Brown W. R., Geller M. J., 2014, ApJ, 793, 122
 Kormendy J., Ho L. C., 2013, ARA&A, 51, 511
 Kozai Y., 1962, AJ, 67, 591

- Kushnir D., Katz B., Dong S., Livne E., Fernández R., 2013, *ApJ*, 778, L37
- Kupi G., Amaro-Seoane P., Spurzem R., 2006, *MNRAS*, 371, L45
- Leigh N. W. C., Geller A. M. 2013, *MNRAS*, 432, 2474
- Leigh N. W. C., Antonini F., Stone N. C., Shara M. M., Merritt D. 2016, *MNRAS*, 463, 1605
- Leigh N. W. C., Stone N. C., Geller A. M., Shara M. M., Muddu H., Solano-Oropeza D., Thomas Y., 2016, *MNRAS*, 463, 3311
- Li G., Naoz S., Kocsis B., Loeb A., 2015, *MNRAS*, 451, 1341
- Lidov M. L., 1962, *Planet. Space Sci.*, 9, 719
- Lu Y., Yu Q., Lin D. N. C., 2007, *ApJ*, 666, L89
- Liu B., Wang Y.-H., Yuan Y.-F., 2017, *MNRAS*, 466, 3376
- Liu B., Lai D., Yuan Y.-F., 2015, *PhRvD*, 92, 124048
- Mandel I., Levin Y., 2015, *ApJ*, 805, L4
- Marchetti T., Contigiani O., Rossi E. M., Albert J. G., Brown A. G. A., Sesana A., 2017, *arXiv*, arXiv:1711.11397
- Martins F., et al. 2006, *ApJ*, 649, L103
- Merritt D. 2013, *Dynamics and Evolution of Galactic Nuclei* (Princeton: Princeton University Press)
- Miller M. C., Hamilton D.P., 2002, *ApJ*, 576, 894
- Naoz S., Kocsis B., Loeb A., Yunes N., 2013a, *ApJ*, 773, 187
- Naoz S., 2016, *ARA&A*, 54, 441
- Perets H. B., 2009, *ApJ*, 698, 1330
- Perets H. B., Subr L. 2012, *ApJ*, 751, 133
- Phinney E. S., 1989, *IAUS*, 136, 543
- Prodan S., Murray N., Thompson T. A., 2013, preprint (arXiv:1305.2191)
- Prodan S., Antonini F., Perets H. B., 2015, *ApJ*, 799, 118
- Rees M. J., 1988, *Nature*, 333, 523
- Ryu T., Leigh N. W. C., Perna R., 2017, *MNRAS*, 470, 3049
- Ryu T., Leigh N. W. C., Perna R., 2017, *MNRAS*, 467, 4447
- Sesana A., Madau P., Haardt F., 2009, *MNRAS*, 392, L31
- Sesana A., Haardt F., Madau P., 2008, *ApJ*, 686, 432-447
- Sesana A., Haardt F., Madau P., 2007, *ApJ*, 660, 546
- Sesana A., Haardt F., Madau P., 2006, *ApJ*, 651, 392
- Soffel M. H., 1989, *S&T*, 78, 382
- Storch N. I., Anderson K. R., Lai D., 2014, *Sci*, 345, 1317
- Springel V., 2005, *MNRAS*, 364, 1105
- Thompson T. A., 2011, *ApJ*, 741, 82
- Wen L., 2003, *ApJ*, 598, 419
- Will C. M., 2014, *PhRvD*, 89, 044043
- Will C. M., 2014, *CQGra*, 31, 244001
- Wu Y., Murray N., 2003, *ApJ*, 589, 605
- Yu Q., Tremaine S., 2003, *ApJ*, 599, 1129

APPENDIX A: SYMPLECTIC ALGORITHM

The advantage of a symplectic algorithm lies in its ability to conserve the Hamiltonian structure of the system. Non-symplectic algorithms control the error to remain within a specified tolerance level, by reducing the time step length. However, if the integration time is long enough, the systematic error will accumulate non-negligibly. The rate of accumulation depends on the adopted time step length. For most gravity integrators, it is adequate to simply adjust the time step length to an acceptable value in order to ensure that the rate of error accumulation is negligible. This is because very long integration times are typically not required. However, to study systems with multi-scale dynamics (e.g., in our four-body system, the spatial scale of the SMBH binary is \sim pc, but the spatial scale of the stellar binary is \sim AU), we need to make sure that we are not failing to resolve important physics, and correctly allowing for the various subtle dynamical processes characteristic of many-body systems to exert their impact on the evolution of the system. This usually requires very long integration times (e.g., the time scale for effect A to operate is much too long for effect B to have any effect, such that the shortest time-scale is what ultimately decides the integration time).

In systems with characteristic multi-scale dynamics, non-symplectic algorithms need extremely long integration times to accurately resolve the relevant physics at the minimum scale. Due to its symmetric numerical format, symplectic algorithms conserve the Hamiltonian structure for much longer integration times. Therefore, over long integration times, symplectic algorithms perform better than non-symplectic algorithms. Unfortunately, the precise symmetry applied to the numerical formatting depends on the adopted time step. This means that only algorithms that use a fixed step length are truly symplectic.

Figure A1 compares the performance of several algorithms in computing long period Keplerian orbits with the adaptive time-step method. Leapfrog and RK2 are second order algorithms. RK4, FR and PEFRL are fourth order algorithms. Leapfrog, FR and PEFRL are symplectic algorithms. RK2 and RK4 are non-symplectic algorithms.

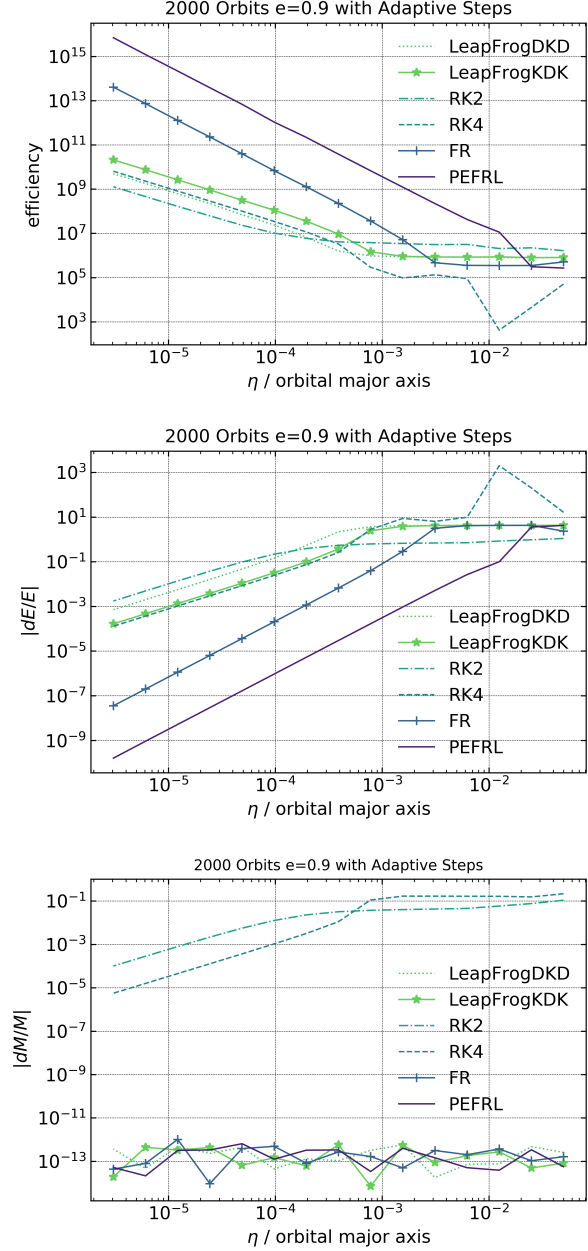


Figure A1. *Top panel:* The total time-steps versus the precision parameter η , which shows the efficiency of the algorithms for the different values of the precision parameter. *Middle panel:* The energy fluctuations as a function η . *Bottom panel:* The angular momentum fluctuations as a function η .